Ann. Geophys., 30, 1285–1295, 2012
www.ann-geophys.net/30/1285/2012/
doi:10.5194/angeo-30-1285-2012

Annales Geophysicae

Geosynchronous magnetic field responses to fast solar wind dynamic pressure enhancements: MHD field model

T. R. Sun[1,2], **C. Wang**[1], **N. L. Borodkova**[3], **and G. N. Zastenker**[3]

[1]State Key Laboratory of Space Weather, National Space Science Center, Chinese Academy of Sciences, Beijing 100080, China
[2]Graduate University of the Chinese Academy of Sciences, Beijing 100049, China
[3]Space Research Institute, Russian Academy of Sciences, Moscow 117997, Russia

Correspondence to: T. R. Sun (trsun@spaceweather.ac.cn)

Received: 6 February 2012 – Revised: 18 June 2012 – Accepted: 4 August 2012 – Published: 27 August 2012

Abstract. We performed global MHD simulations of the geosynchronous magnetic field in response to fast solar wind dynamic pressure (P_d) enhancements. Taking three P_d enhancement events in 2000 as examples, we found that the main features of the total field B and the dominant component B_z can be efficiently predicted by the MHD model. The predicted B and B_z varies with local time, with the highest level near noon and a slightly lower level around mid-night. However, it is more challenging to accurately predict the responses of the smaller component at the geosynchronous orbit (i.e., B_x and B_y). In contrast, the limitations of T01 model in predicting responses to fast P_d enhancements are presented.

Keywords. Magnetospheric physics (Solar wind–magnetosphere interactions)

1 Introduction

The magnetospheric magnetic field is an essential parameter determining the dynamics of the solar wind–magnetospheric coupling system. Therefore, a reliable magnetic field model is essential in geospace investigations. Recent development of the space weather forecast also requires an accurate prediction of the magnetic field in our surrounding environment.

Global MHD simulation provides a convenient access to the magnetic field in the three-dimensional magnetosphere. However, the predictive ability of the MHD magnetic field model should be carefully evaluated before its application. Validation studies of numerical simulation models have become a primary focus recently. Long period (3 yr) characteristics of the modeled magnetic field were consistent with Cluster spacecraft observation according to Daum et al. (2008). Storm time geosynchronous magnetic fields detected by GOES satellite, varying on a time scale of hours, were compared with several MHD field models (e.g., Huang et al., 2006; Pulkkinen et al., 2010; Rastatter et al., 2011). The under-stretched nightside field lines during storm time can be improved by inclusion of a ring current model. Magnetic field evolutions during substorms, with a characteristic time of about half an hour, were also investigated by observation and the corresponding simulation (e.g., Raeder et al., 2001; Wiltberger et al., 2000). However, to our knowledge, the validation works are scarcely carried out to examine the detailed features of the magnetic field transient variations on a time scale of minutes. Recognizing that future space weather investigations will probably progress towards a higher accuracy within a smaller temporal scale, similar to meteorologic development, this paper focuses on detailed validation of the MHD field model.

Fast solar wind P_d enhancements (sharp increase within $\sim$2 min) introduce compressional wave to the magnetosphere, which enhances the dayside magnetic field and causes complicated variations on the nightside (e.g., Lee and Lyons, 2004; Villante and Piersanti, 2008; Andreeova et al., 2011; Sun et al., 2011). The typical time duration of the geosynchronous magnetic field responses are within $\sim$8 min according to GOES measurement. These transient events thus provide a good opportunity to evaluate the immediate responsiveness of the MHD field model. Aside from the validation purpose, a reliable magnetic field model also assists space physics investigations. After fast solar wind P_d

enhancements, various processes, in addition to the magnetic field changes, are also aroused in the magnetosphere-ionosphere system such as traveling convection vortices (TCV) (e.g., Lam and Rodger, 2004; Yu and Ridley, 2009), particle energization associated with magnetic field compression (Shi et al., 2009; Turner and Li, 2008), and even substorm related activities (Yue et al., 2010). Investigations on some of these processes depend on a reliable and accurate field model.

Another category of the magnetic field models is the empirical ones based on observation (e.g., the series of Tsyganenko models: Tsyganenko and Stern, 1996; Tsyganenko, 2002, and so on). They predict the magnetic field by representing the external part of the total field as the sum of contributions from major magnetospheric current systems, estimated from a considerable amount of satellite measurements. Unlike the physics-based MHD models which require certain calculation time, the empirical ones can predict the magnetic field almost instantaneously. Consequently, some researchers might view the empirical models as the top priority whenever a field model is needed, reluctant to bother with the numerical calculation. However, each model has its own optimum range of applications. For instance, during storm times, the empirical models perform well for weak storms, while the MHD models are better for strong ones (Rastatter et al., 2011). Therefore, what should be carefully evaluated before application is whether the empirical model is appropriate to describe the transient magnetic field variations at the geosynchronous orbit, where the magnetic field is continuously monitored.

The data sources and the MHD model used in this paper are briefly introduced in Sect. 2. By analyzing three typical events occurring in 2000, Sect. 3 reports the detailed performance of the MHD magnetic field model after fast solar wind P_d enhancements. Section 4 presents discussions on the metrics and the model discrepancies. Also shown in this section are the limitations of the T01 model in describing the magnetic field responses to fast P_d enhancements. Finally, the summary is given in Sect. 5.

2 Data sources and MHD code

The solar wind parameters used as the input of the MHD code are provided by the Wind spacecraft. We obtained the 3 s resolution interplanetary magnetic field (IMF) and plasma data observed by the Magnetic Fields Investigation (MFI) and the 3-D Plasma Analyzer (3DP) from the Coordinated Data Analysis Web (CDAWeb). To determine the normal of the interplanetary (IP) discontinuity, the three-spacecraft timing method was used (Riazantseva et al., 2003), and the solar wind data measured by IMP 8, Interball-1, and ACE were also examined. The geosynchronous magnetic field was recorded each minute by GOES-08 and -10 (also from CDAWeb).

Variations of the geosynchronous magnetic field were studied by using a global MHD simulation code developed by Hu et al. (2007). Numerical method applied in the code is an extended Lagrangian version of the piecewise parabolic method (PPMLR) (Colella and Woodward, 1984). The MHD equations are solved in Cartesian coordinate system, with a numerical box extending from 30 to $-300\,R_E$ along the x-axis and from -150 to $150\,R_E$ in the y- and z-directions. A $0.4\,R_E$ uniform mesh is chosen in the cube defined by $-10 \le x, y, z \le 10\,R_E$, and the grid spacing outside it increases gradually along each axis. As an example, the code with a finer spatial resolution ($0.2\,R_E$ minimum grid spacing) was also run for the 4 November 2000 event to show the effects of the numerical mesh. As will be discussed in Sect. 3.3, the spatial resolution has no apparent influence on the results, and hence the $0.4\,R_E$ grid is used for the present study. The inner boundary of the magnetospheric domain is a spherical shell with a radius of $3\,R_E$. Coupled with this boundary, the ionosphere is assumed to be a spherical shell with a uniform Pedersen conductance and a zero Hall conductance. Time resolution for the simulation results in this study is about 28 s.

The main field of the Earth is assumed as a dipole in this code with its moment anti-parallel to the z-axis, which indicates that the MHD equations are solved in the SM coordinate system. Direct comparison between GOES observation (in GSM) and the numerical output (in SM) implicates that the dipole tilt angle is approximated zero. Although the dipole tilt averaged zero near the equinox, it can reach more than 30° near the summer and winter solstices. Therefore, to include the effect of nonzero dipole tilt, we first convert the observed solar wind conditions from GSE to SM to prepare the input parameters of the code. Then, after running the code in SM, the numerical results are converted back to the GSM coordinate system. Input parameters are based on the real-time observation of Wind. Specifically, to obtain a quasi-steady initial state, we calculated more than 5 h (physical time) using the averaged upstream parameters of the discontinuity as the input. Afterward, real-time solar wind parameters were introduced at the inflow boundary about 6 min before Wind detected the discontinuity. B_x at the inflow boundary was set 0 initially and then changed each time step to ensure the divergence free condition for the magnetic field.

3 The MHD magnetic field model in response to sudden P_d enhancements

This section presents GOES observation and MHD simulation for three events with abrupt solar wind P_d enhancements.

3.1 The 14 August 2000 event

Figure 1 shows solar wind conditions for the 14 August 2000 event observed by Wind, with the number density (N), velocity, IMF and temperature portrayed by the black lines from the top to the bottom panels. The vertical dashed lines mark the passage of the discontinuity at about 22:16 UT. Also plotted in this figure are available solar wind parameters provided by ACE, Interball-1, and IMP 8. To better show the P_d variations in one figure, ACE, Interball-1, and IMP 8 data were shifted by 41, 2.5, and 2 min, respectively. Since ACE was far away from the other satellites (positions shown in Fig. 1), the start time of the P_d enhancement recorded by Wind, Interball-1, and IMP 8 was selected to calculate the discontinuity normal by using the three-spacecraft timing method. The normal was (−0.45, 0.84, −0.31) GSE with an error of 17.9°. The first two panels of Fig. 1 reveal that the detected P_d structures were similar at all spacecrafts, indicating insignificant evolution of the shock from ACE toward Wind. Therefore, based on the consideration of a higher temporal resolution, Wind data was chosen as the input of the MHD code.

GOES-08 at dusk (17.1 LT) and GOES-10 near noon (13.3 LT) both observed the magnetic field responses, shown by the star symbols in Fig. 2. The fourth and third panels show that the magnetic field strength and the dominant component B_z at both satellites increased abruptly after the disturbance arrival. The subsequent decrease of B and B_z following the compression tends to be attributed to the gradual drop back of the enhanced P_d downstream of the discontinuity shown by Fig. 1. The B_x and B_y magnitude at GOES-08 as well as the B_y magnitude at GOES-10 increased in response to the P_d enhancement, partly falling back afterwards. B_x at GOES-10 shows a bipolar variation. Compared with GOES data, the red diamonds in Fig. 2 depict the modeled magnetic field, which provides a preliminary visual assessment of the MHD model performance. The MHD magnetic field model captures the sudden increase of B and B_z at both satellites quite well, without substantial underestimation of the increment. Besides, the subsequent decreases of the modeled B and B_z almost exactly follow the observed tendency near noon. This trend is also partly revealed by the modeled B and B_z at GOES-08 near dusk, although the discrepancy is larger than that of GOES-10. The B_x and B_y magnitude were not so significant compared to the largest component B_z. Nevertheless, the MHD model is able to reproduce about 50 % of the compressional effect of the P_d enhancement at GOES-08 for B_x, B_y and at GOES-10 for B_y. The numerical simulation fails to predict the observed B_x response at GOES-10.

In order to quantitatively measure the performance of the MHD field model, two main metrics are applied. Firstly, to measure the maximum response ability of a model after fast solar wind dynamic pressure enhancements, P_{dB} is defined as the ratio of the relative variations of the modeled and observed magnetic field:

$$P_{dB} = \frac{(B_{mex} - B_{m0}) \cdot B_{o0}}{(B_{oex} - B_{o0}) \cdot B_{m0}}, \quad (1)$$

B_{mex} and B_{oex} (B_{m0} and B_{o0}) represent the extrema (quasi-steady value) of the modeled and observed B right after (before) the arrival of the solar wind disturbance. A perfect magnetic field model corresponds to $P_{dB} = 1$. Table 1 lists P_{dB} values for the MHD and T01 (discussed in the next section)

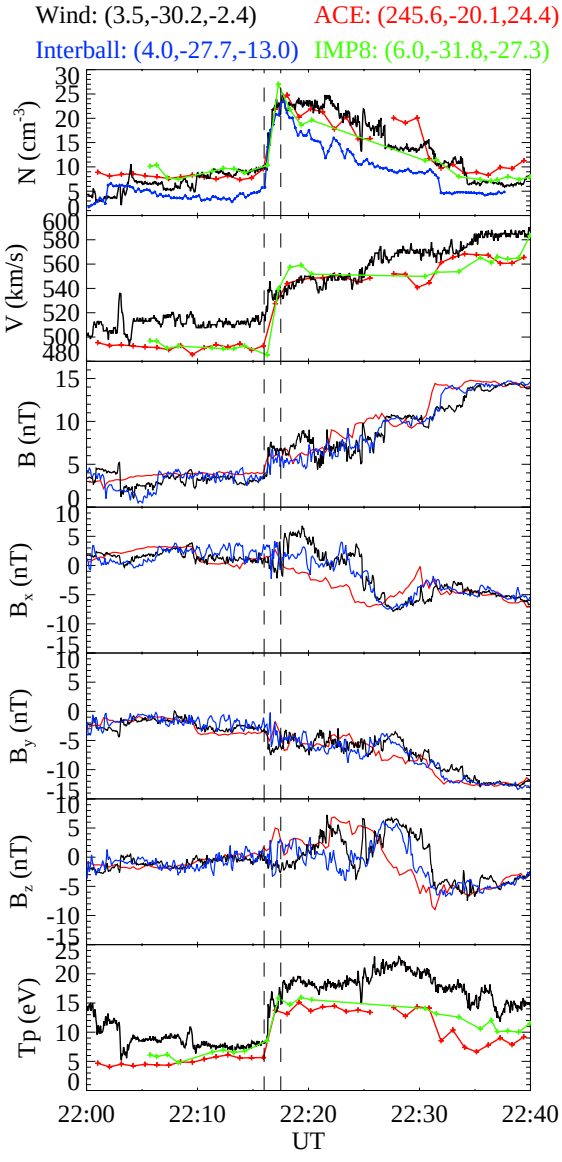

Fig. 1. Solar wind conditions in the GSE coordinate system for the 14 August 2000 event. From the top to the bottom, the panels show the density, speed, IMF and temperature observed by Wind. Available parameters detected by ACE, Interball-1 and IMP 8 are also plotted, shifted by 41, 2.5, and 2 min, respectively. On the top of the figure, positions of the four satellites are listed. The vertical dashed lines mark the sudden enhancement of P_d.

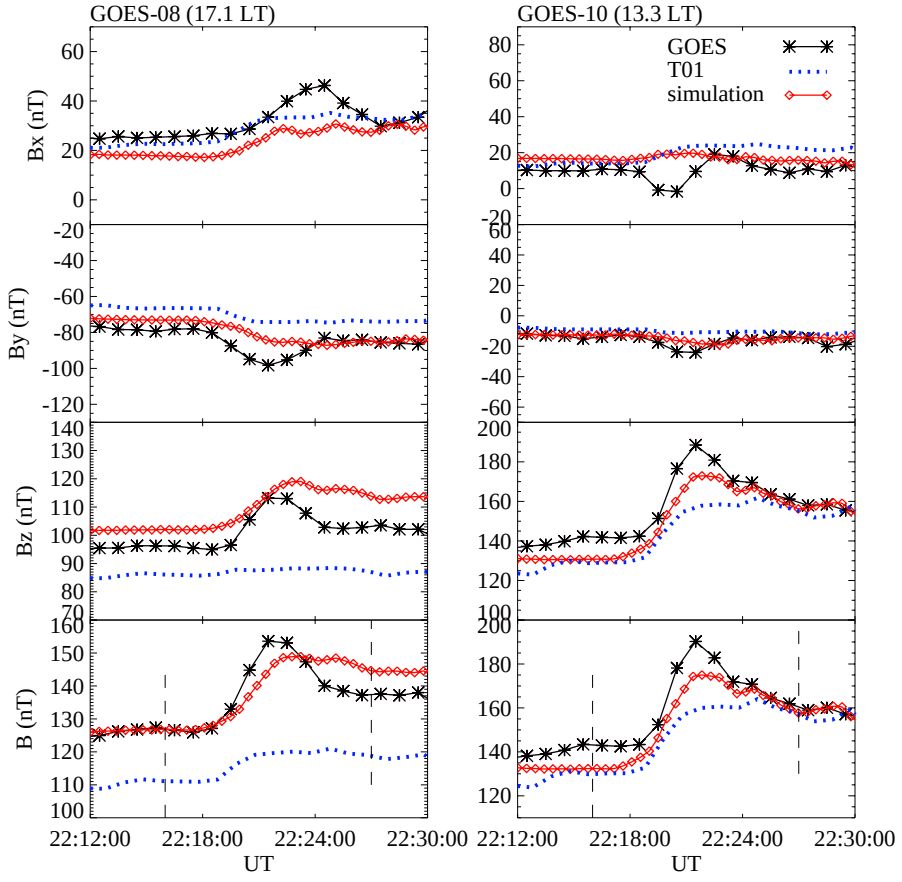

Fig. 2. Magnetic field at GOES-08 (left) and -10 (right) for the 14 August 2000 event. The stars denote the magnetic field observed by GOES, and the blue dotted lines are predicted by T01 model. Simulation results are shown by the red diamonds. The vertical dashed lines in the fourth panels show the time interval chosen to do the quantitative analyses.

Table 1. P_{dB} values, defined by Eq. (2), of the MHD and T01 field models respectively for the three presented events.

Date	14 August 2000		6 June 2000		4 November 2000	
GOES	-08	-10	-08	-10	-08	-10
P_{dB} (MHD)	0.85	0.93	0.71	0.81	0.70	1.0
P_{dB} (T01)	0.37	0.70	0.63	0.61	2.5	−0.59

models. It is evident that for the 14 August 2000 event, the maximum response capability of the MHD field model is close to the satellite measurement at both places. This quantitatively confirms the conclusion made by the visual assessment of Fig. 2: the MHD field model captures the increase of B without remarkably underrating the amount of field compression.

The other applied metric is the normalized root mean square (RMS_n), defined as

$$RMS_n = \frac{\sqrt{< (B_m - B_o)^2 >}}{\sqrt{< B_o^2 >}}, \quad (2)$$

where B_m and B_o denote the modeled and observed magnetic field, respectively. The perfect value for RMS_n is 0, indicating that the model exactly agrees with observation. In order to include the magnetic field information upstream and downstream as well as during the response process, $3 \sim 5$ min before/after the apparent variation of B is selected as the start/end time to calculate RMS_n. To the left side of Table 2, RMS_n between observation and MHD simulation are listed for the 14 August 2000 case, calculated during the time interval marked by the vertical dashed lines in Fig. 1. It is revealed that the RMS_n values of B (B_z) are smaller than 0.06 (0.09) for the MHD field model at both satellites, showing well predicted responses. RMS_n of B_x and B_y at GOES-08 and B_y at GOES-10 vary between 0.094 to 0.31, which indicate a somewhat reasonable consistency. It is noted that the metric RMS_n should be carefully utilized when the average of the detected field approximates zero, as it tends to magnify small discrepancies if the denominator of Eq. (2) is close to zero. This seems one of the contributing factors for the large RMS_n of B_x at GOES-10. Another possible cause tends to

be a relatively weak predictability of the MHD field model when describing transient variations of the smaller field component.

3.2 The 6 June 2000 event

Another P_d enhancement event was measured by Wind on 6 June 2000. The solar wind parameters observed by Wind, ACE, IMP 8 and Interball-1 are shown in Fig. 3, in similar format as Fig. 1. During the time interval marked by the vertical dashed lines, P_d remained stable for about 3 min (at Wind) between two successive enhancements. The normal values of both discontinuities were calculated by using the observations of Wind, Interball-1, and IMP 8. As the two discontinuities cannot be discriminated by the plasma data at IMP 8, the 320 ms magnetic field data was also analyzed to estimated the onset time. The normal was determined as (−0.74, −0.67, −0.05) GSE with an error of 6.8° for the first P_d enhancement, and (−0.70, −0.66, 0.26) GSE with an error of 8.0° for the second one.

In response to the P_d enhancements, GOES-08 near noon (12.0 LT) and GOES-10 at the dawn side (7.8 LT) observed sudden increase of B and B_z (the dominant component) as well as a subsequent decrease, depicted by the stars in Fig. 4. Interestingly, although the solar wind P_d remained unchanged for several minutes between two sharp enhancements (Fig. 3), the magnetic field strength and the dominant component B_z kept increasing without any break. Actually, the typical rise time duration of the magnetic field responses to sharp P_d enhancement varies within ∼8 min, depending on the normal of the discontinuity (Guo et al., 2005). The more apparently the discontinuity normal deviates from the Sun–Earth line, the longer the response time is. Consequently, the tilted normal in this event indicates that during the short P_d platform (lasted ∼3 min), the magnetospheric magnetic field might keep increasing in response to the first P_d enhancement, resulting in a continuously rising profile of B. B_x and B_y magnitudes at both satellites showed immediate enhancements after the disturbance arrival.

The red diamonds in the third and fourth panels of Fig. 4 reveal a consistency of the B_z and B responses between the MHD field model and observation at both satellites. Remarkably, the MHD field model is able to reproduce the continuous compression of the magnetic field after the arrival of two successive P_d enhancements. For the B_x and B_y components which were less significant compared with B_z, the MHD field model can partly reveal their compressional responses according to Fig. 4, except the B_y variation at GOES-08. Table 1 shows that the P_{dB} values for the MHD model approximate 1 at both satellites, implying a maximum response capability close to reality. Quantitative evaluation of the model performance is further demonstrated by Table 2. The RMS_n values of B (B_z) for the MHD field model are no larger than 0.08 (0.13) at both satellites, indicating a good agreement with observation. RMS_n values of B_x and B_y at GOES-10 and B_x at GOES-08 suggest a somewhat reasonable model prediction. The relatively large RMS_n of B_y at GOES-08 implies that it seems more difficult for the MHD field model to precisely predict responses of the minor components.

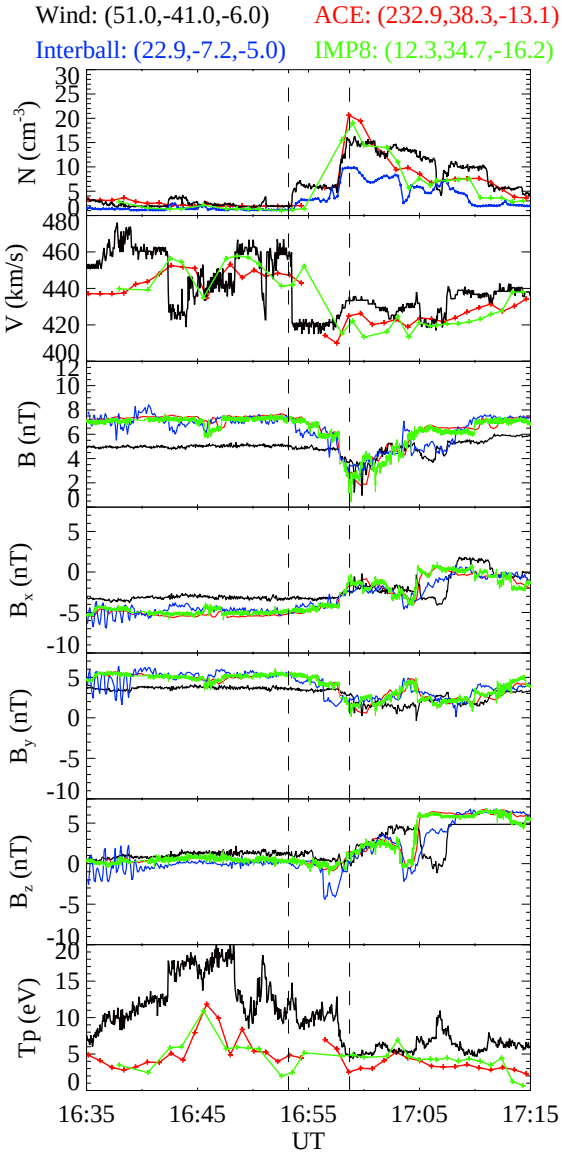

Fig. 3. Solar wind conditions in the GSE coordinate system for the 6 June 2000 event. The parameters are shown in a similar format as in Fig. 1. ACE, Interball-1 and IMP 8 measurements were shifted by 67, 0.83, and 9 min, respectively.

3.3 The 4 November 2000 event

The third P_d enhancement event, observed by Wind (at (65.1, −138.6, 6.5) R_E GSE) on 4 November 2000, is depicted in Fig. 5. This is an IP shock event, and the shock normal determined by the Rankine-Hugoniot-08 methods is (−0.93,

Table 2. Normalized root mean square (RMS_n) and prediction efficiency (PE, defined and discussed in Sect. 4.1) between GOES observation and MHD/T01 field model for the three studied events.

date	14 August 2000				6 June 2000				4 November 2000			
GOES	-08		-10		-08		-10		-08		-10	
model	MHD	T01	MHD	T01	MHD	T01	MHD	T01	MHD	T01	MHD	T01
$RMS_n\_B_x$	0.31	0.18	0.88	1.0	0.43	1.1	0.065	0.093	5.3	3.6	0.046	0.12
$RMS_n\_B_y$	0.094	0.19	0.20	0.43	2.9	0.78	0.22	0.34	0.14	0.23	0.20	0.51
$RMS_n\_B_z$	0.086	0.16	0.056	0.12	0.045	0.085	0.13	0.050	0.096	0.098	0.055	0.10
RMS_n_B	0.041	0.17	0.053	0.11	0.044	0.081	0.073	0.047	0.11	0.052	0.035	0.098
PE_B_x	−0.94	0.38	−1.5	−2.3	0.56	−1.8	−0.39	−1.9	−27.0	−12.0	0.46	−2.9
PE_B_y	−0.32	−4.5	0.30	−2.4	−10.0	0.21	−0.38	−2.4	0.31	−0.84	0.63	−1.3
PE_B_z	−0.76	−5.1	0.70	−0.30	0.80	0.31	−2.1	0.51	−34.	−36.0	0.10	−2.1
PE_B	0.68	−4.4	0.73	−0.22	0.82	0.38	0.099	0.63	−17.0	−2.8	0.56	−2.4

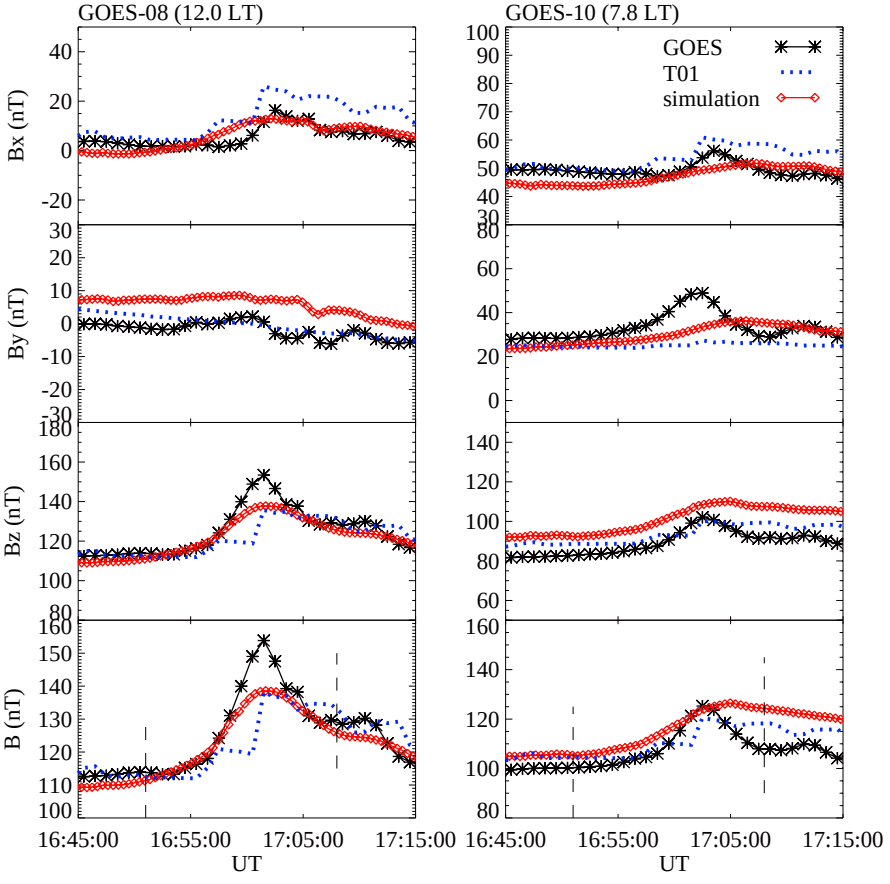

Fig. 4. Magnetic field at GOES-08 (left) and -10 (right) for the 6 June 2000 event. Figure formats are similar to Fig. 2.

−0.19, 0.33) GSE with an error of 7.6° based on the CfA online shock database (http://www.cfa.harvard.edu/shocks/).

Variations of the geosynchronous magnetic field were observed by GOES-08 (21.5 LT) on the nightside and GOES-10 (17.7 LT) near dusk, shown by the stars in Fig. 6. The magnetic field responded differently at different local times: it rose at the dusk-side yet dropped in the mid-night sector, which was discussed in detail by Wang et al. (2010). The B_x magnitude enhanced while the B_y magnitude decreased at both satellites. All the above mentioned response features are well reproduced by MHD simulation, illustrated by the red diamonds in Fig. 6. Visual assessment of the MHD field model reveals a good agreement with satellite detection, despite the slightly larger B_x and B_z magnitude on the nightside

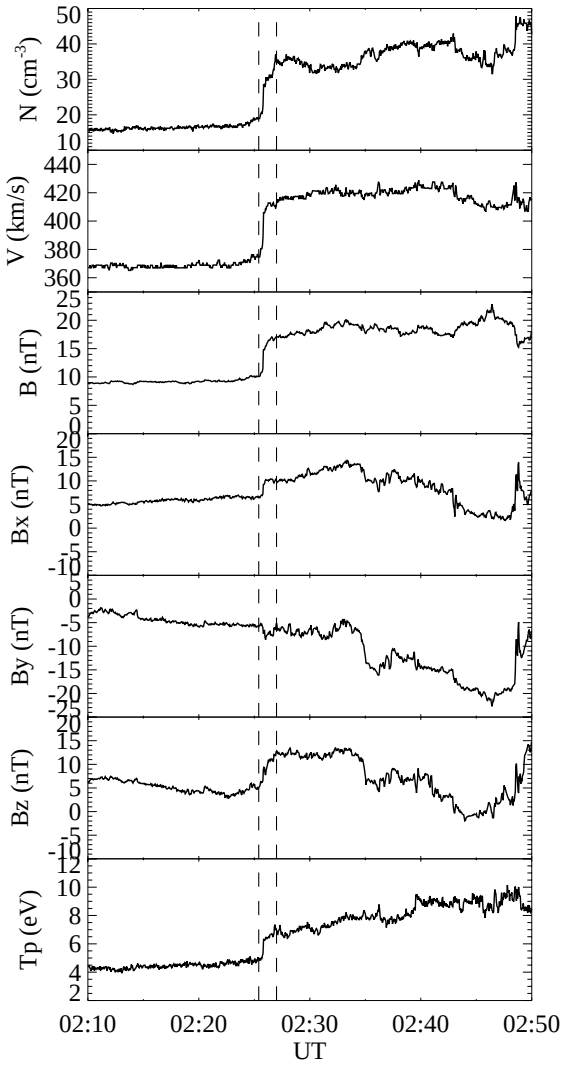

Fig. 5. Solar wind conditions in the GSE coordinate system for the 4 November 2000 event. The parameters are shown in the same format as in Fig. 1.

at GOES-08. The code with a finer spatial resolution (0.2 R_E) was also run to show the effects of numerical mesh. Figure 6 reveals that no significant differences exist between the 0.4 R_E (red diamonds) and 0.2 R_E (green crosses) resolution results. Consequently, discussions in this paper are all based on the 0.4 R_E resolution results. P_{dB} listed in Table 1 measures the maximum response capability of the MHD field model. It is manifested that the modeled field is compressed at a ratio close to reality near dusk, whereas the decrease of the magnetic field is slightly underestimated on the nightside. Quantitative measurements presented by Table 2 show an efficient prediction of B (B_z), as the RMS_n values are no larger than 0.11 (0.096). Nevertheless, nightside prediction error is larger than that near dusk. B_x and B_y at GOES-10 and B_y at GOES-08 are also reasonably predicted by the MHD model. The higher RMS_n value of B_x at GOES-08 implies a relatively large deviation from observation.

4 Discussion

4.1 Prediction efficiency

In addition to the visual assessment and the two main metrics (i.e., P_{dB} and RMS_n) utilized to evaluate the model performance, another method frequently applied in the literature is the prediction efficiency (PE), defined as

$$PE = 1 - \frac{\langle (B_m - B_o)^2 \rangle}{\sigma_o^2}, \quad (3)$$

where σ_o^2 is the variance of the satellite measurements. A perfect prediction model has a PE value of 1. It is noted that although PE serves as a good metric when the magnetic field has large variations, such as the ground and geosynchronous magnetic field variations during storms (e.g., Pulkkinen et al., 2010), it tends to exaggerate a small inconsistency if the field responses (the denominator) are weak. Usually, B responds more apparently near noon (typically tens of nT) than in the nightside (usually several nT) (Lee and Lyons, 2004), and the variations of the smaller components (B_x and B_y) are weaker. Therefore, PE might have some limitations in validating the model responses around the mid-night and for the minor components. But still, listing the PE values can help to give further impression of the model performance. Judging from the three studied events, PE_B is closest to 1 near noon, as shown by Table 2, which indicates a good predictive capability. It decreases toward dawn and dusk, implying that the model performance near the terminator is at a slightly lower level compared with the local noon.

4.2 Summary of the model performance and analyses of the discrepancies

As shown by the analyses of the three P_d enhancement events, the MHD field model is able to predict the main response features of B and the dominant component B_z at the geosynchronous orbit. Firstly, the modeled field follows the main response tendency of the observed B and B_z. Moreover, the sudden increase (or decrease) of B and B_z is relatively adequately reflected by the MHD field model, which demonstrates a maximum response capability close to reality. In addition, the MHD field model well reproduces detailed response features such as the sustained compression during two successive P_d enhancements. The above analyses also suggest that the level of the MHD model performance is highest near noon and slightly decreases toward mid-night. For smaller components of the magnetic field at the geosynchronous orbit (B_x and B_y), the variations are sometimes difficult to precisely predict.

Besides the three presented cases, we have simulated several other P_d enhancement events such as the 7 November

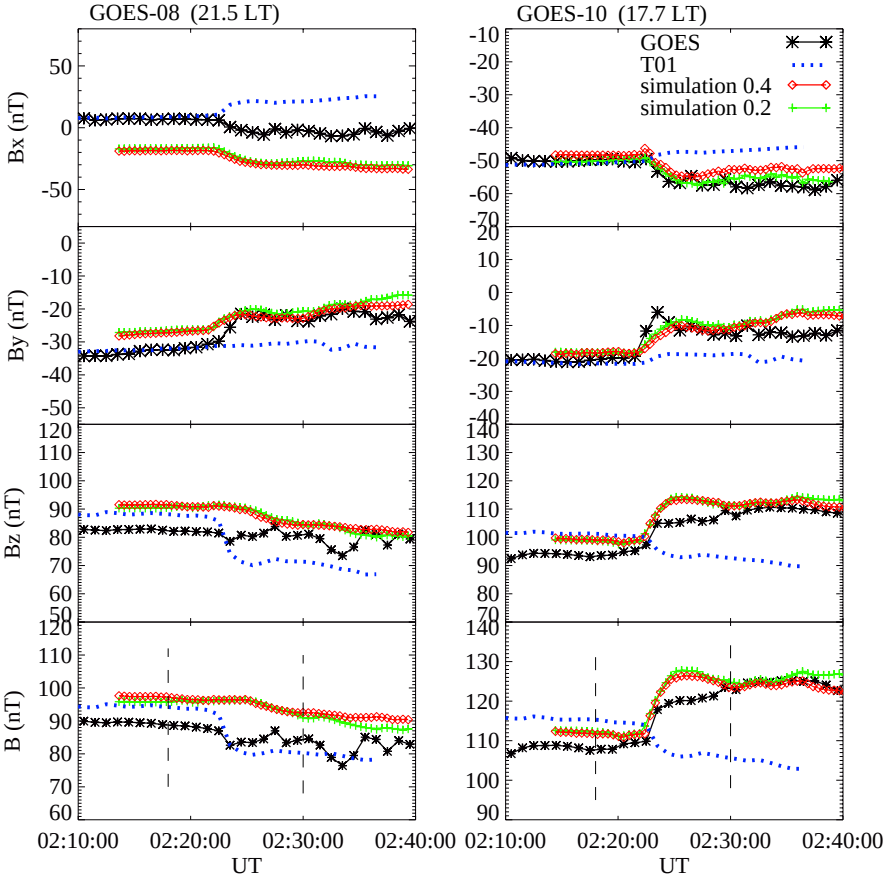

Fig. 6. Magnetic field at GOES-08 (left) and -10 (right) for the 4 November 2000 event. Figure formats are similar to Fig. 2. Green crosses (red diamonds) show the results with 0.2 (0.4) R_E spacial resolution.

2004 event. Model performances for all these events are similar to those discussed above, and hence the main conclusions of the paper are not event dependent based on the simulation by far.

Although the MHD code presents an efficient prediction in general, discrepancies exist between simulation and observation. Many aspects may be responsible for these discrepancies. Firstly, errors exist at the inflow boundary of the simulation code. As the IP discontinuities may have some evolutions when traveling between the Wind spacecraft and the inflow boundary of the code ($x = 30\,R_E$), directly using Wind observation as the input parameter might introduce errors to the whole solar wind-magnetospheric system. Normals of the discontinuities are difficult to be precisely determined as well. Take the 4 November 2000 event as an instance: the CfA shock database presents eight normals determined by four different methods (i.e., Magnetic Coplanarity, Velocity Coplanarity, Magnetic-Velocity Coplanarity (mixed) and the Rankine-Hugoniot method), and the maximum differences can reach as high as 50°. B_y near dawn and dusk may be more sensitive to the accuracy of the estimated discontinuity normal (n_x, n_y, n_z), especially the value of n_y. This is a possible reason for the discrepancy between the simulated B_y and GOES-08 detection for the 14 August 2000 event (Fig. 2). Secondly, assumptions of the MHD code also tend to result in some discrepancies. To avoid long calculation time caused by large Alfven velocity near Earth, an inner boundary is introduced at $r = 3\,R_E$ and the inner magnetosphere is coupled with a simplified ionosphere. This process may lead to an inaccurate Region 1 current system which affects the geosynchronous magnetic field (B_x or B_z). Thirdly, the global MHD model fails to reproduce a realistic ring current, which introduces errors to the modeled field, especially the nightside B and B_z.

4.3 Possible influences of the foreshock region

As seen from Figs. 1, 3, and 5, the IMF direction was mainly parker spiral ($B_x/B_y < 0$) for all three events during the interested time interval (i.e., about 6 min before and after Wind observed the discontinuity), implying the existence of a foreshock upstream of the Earth's bow shock on the dawn side. Wind spacecraft was located in this region during the

14 August and 6 June 2000 events. As the backstreaming particles in the foreshock region can sometimes modify the background solar wind parameters, we briefly analyze the possible influence of the foreshock on the input parameters of the code. Firstly, during the interested time interval, foreshock-related structures which can lead to striking P_d variations, such as the foreshock cavities (e.g., Sibeck et al., 2002) and hot flow anomalies (Schwartz et al., 1985), cannot be discerned from Wind data. Secondly, the possible deceleration of the solar wind in the foreshock region is only 7–10 km s^{-1} on average (Bame et al., 1980), indicating an insignificant modification of P_d. Thirdly, the reported blurring of the IP shock front in the foreshock region (Prech et al., 2009) was not observed in the present study. Therefore, the foreshock signatures which may substantially vary the input parameters have not been recognized, and the MHD results cannot reveal the foreshock effects.

GOES observation may contain some information on the geoeffectiveness of the foreshock structures, since such structure may exist even though Wind was not located in a proper position to observe it. This seems an additional factor potentially responsible for the discrepancy between numerical and observational results. We analyze features of this discrepancy to discuss whether the foreshock is crucial for the events studied here. Foreshock signature which can lead to striking P_d variations, such as the foreshock cavity, is generally characterized by a region of depressed P_d bounded by enhancements on one or both sides. Its effect on the dayside geosynchronous magnetic field is the decrease of field strength bounded by enhancements according to Sibeck et al. (2000). Therefore, if foreshock played a significant role in the present study, there would exist a time interval during which the observed magnetic field was apparently smaller than the simulated one, while larger than it on the leading or/and trailing sides. However, such time interval cannot be discerned from the right column of Fig. 2 and the left one of Fig. 4, which both show field responses near local noon. Consequently, we do not consider the foreshock effect crucial for the events studied in this manuscript.

Nevertheless, the possibility that foreshock-related structures may occur and play a significant role during other solar wind P_d enhancement events does exist. Although it might be important, the precise prediction of foreshock effect is a challenge for the present model, since the foreshock signatures can neither be thoroughly specified at the inflow boundary of the code due to limited solar wind monitors nor be reproduced self-consistently by the one-fluid MHD code. Future investigations on this topic may involve the coupling between the present code and a hybrid one.

4.4 Limitations of T01 model in response to fast solar wind P_d enhancements

Among the four Tsyganenko models frequently used in the literature (T89, T96, T01 and TS04), the observational database for T01 has a relatively high time resolution of 5 min. Also considering that the geomagnetic conditions were relatively quiet without storms for the three events analyzed in this paper ($Dst > -20$), this subsection selects the T01 model as a typical instance to compare the performance of the empirical and MHD field models in response to P_d enhancements. Time evolutions of the magnetic field predicted by the T01 model for the studied events are portrayed by the blue dotted lines in Figs. 2, 4, and 6. P_{dB} and RMS_n are listed in Tables 1 and 2, respectively. Overall, the T01 model reproduces the main characteristics of the responses under some circumstances. However, there are exceptions:

1. The maximum response capability of T01 model sometimes departs apparently from observation. The left side of Fig. 2 shows that for the 14 August 2000 event, the largest component B_z remains unchanged after the disturbance arrival, apparently diverging from the detection of GOES-08. The slightly elevated B results from the weak increases of B_x and B_y magnitudes, which are less important components. RMS_n of B and B_z in Table 2 are relatively high, indicating noticeable deviation from observation. The maximum response ability of T01 model at GOES-08 is only about one third of observation, according to P_{dB} shown in Table 1. Even for those circumstances when the T01 model reasonably agrees with observation (GOES-10 on 14 August 2000; GOES-08 and -10 on 6 June 2000), it predicts 70 % of the observed increase at most. As to the 4 November 2000 event, T01 predicts a decrease amplitude of B a bit larger than observation at GOES-08. By contrast, the maximum response ability of the MHD field model is relatively stable for all three cases, with P_{dB} varying between 70 % and 100 %.

2. The T01 model leads to an opposite response trend in some cases. For the 4 November 2000 event, compression of B near dusk was detected by GOES-10. However, the T01 model predicts decrease of B, as seen from Fig. 6 and the negative P_{dB} value in Table 1. This disagreement exposes the potential unreliability of the T01 model in predicting the field response to fast P_d enhancements. On the other hand, the MHD field model predicts the observed tendency efficiently.

3. Detailed variations of the magnetic field may not be captured by the T01 model. Although the solar wind P_d remained unchanged for $\sim$3 min between two successive enhancements on 6 June 2000, the observed magnetic field strength kept increasing without any break. Unlike the MHD model, the T01 model fails to reproduce this detailed feature as it changes with the solar wind condition instantaneously.

Considering all of the above, the T01 model is not the first choice for space weather predictions and magnetospheric investigations in response to sharp solar wind P_d enhancements.

5 Summary

By presenting the MHD magnetic field model for three fast solar wind P_d enhancement events occurring in 2000 as examples, this paper shows efficiently predicted responses of the total field B and the dominant component B_z at the geosynchronous orbit. The modeled field follows the main response tendency (increase or decrease) of the observed B and B_z, and relatively adequately reveals the response amplitude without substantial underestimation. Remarkably, the detailed response features such as the continued compression between two successive P_d enhancements are also captured by the MHD field model. The model performance in predicting B and B_z varies with local time, with the highest level near noon and a slightly lower level around mid-night. The relatively larger B and B_z errors on the nightside, as shown by Fig. 6, might be improved by inclusion of a ring current model in future works. Besides, for smaller components of the magnetic field at the geosynchronous orbit (B_x and B_y), it is more challenging to accurately predict their responses. The MHD field model sometimes deviates from the observed B_x and B_y, given that the smaller variations tend to be apparently affected by model assumptions such as the simplified ionosphere. Performance of the T01 model is also discussed in this paper. Unlike the stable behavior of the MHD field model, T01 sometimes fails to reproduce the observed response of the dominant component B_z, or even predicts an opposite trend. The MHD magnetic field model also outperforms T01 in revealing the detailed response features. Therefore, for space weather forecast and geospace investigations under the condition of fast solar wind P_d enhancements, the MHD magnetic field model tends to be a reliable choice.

Acknowledgements. The authors are grateful for the use of data from CDAWeb and the shock normal information from Harvard CfA Shock Database. This work was supported by 973 program 2012CB825602, NNSFC grants 40921063, 40831060, grant RFFI 10-02-01063, and in part by the Specialized Research Fund for State Key Laboratories of China.

Topical Editor R. Nakamura thanks two anonymous referees for their help in evaluating this paper.

References

Andreeova, K., Pulkkinen, T. I., Juusola, L., Palmroth, M., and Santolík , O.: Propagation of a shock-related disturbance in the Earth's magnetosphere, J. Geophys. Res., 116, A01213, doi:10.1029/2010JA015908, 2011.

Bame, S. J., Asbridge, J. R., Feldman, W. C., Gosling, J. T., Paschmann, G., and Sckopke, N.: Deceleration of the solar wind upstream from the earth's bow shock and the origin of diffuse upstream ions, J. Geophys. Res., 85, 2981, doi:10.1029/JA085iA06p02981, 1980.

Colella, P. and Woodward, P. R.: The piecewise parabolic method (PPM) for gas-dynamical simulations, J. Comput. Phys., 54, 174–201, 1984.

Daum, P., Denton, M. H., Wild, J. A., Taylor, M. G. G. T., Šafránková, J., and Hayosh, M.: A general Cluster data and global MHD simulation comparison, Ann. Geophys., 26, 3411–3428, doi:10.5194/angeo-26-3411-2008, 2008.

Guo, X. C., Hu, Y. Q., and Wang, C.: Earth's magnetosphere impinged by interplanetary shocks of different orientations, Chin. Phys. Lett., 22, 3221–3224, 2005.

Hu, Y. Q., Guo, X. C., and Wang, C.: On the ionospheric and reconnection potentials of the earth: Results from global MHD simulations, J. Geophys. Res., 112, A07215, doi:10.1029/2006JA012145, 2007.

Huang, C.-L., Spence, H. E., Lyon, J. G., Toffoletto, F. R., Singer, H. J., and Sazykin, S.: Storm-time configuration of the inner magnetosphere: Lyon-Fedder-Mobarry MHD code, Tsyganenko model, and GOES observations, J. Geophys. Res., 111, A11S16, doi:10.1029/2006JA011626, 2006.

Lam, M. M. and Rodger, A. S.: A test of the magnetospheric source of traveling convection vortices, J. Geophys. Res., 109, A02204, doi:10.1029/2003JA010214, 2004.

Lee, D.-Y. and Lyons, L. R.: Geosynchronous magnetic field response to solar wind dynamic pressure pulse, J. Geophys. Res., 109, A04201, doi:10.1029/2003JA010076, 2004.

Prech, L., Nemecek, Z., and Safrankova, J.: Influence of the foreshock of the Earth's bow shock on the interplanetary shock propagation during their mutual interaction, Earth Planets Space, 61, 607–610, 2009.

Pulkkinen, A., Rastätter, L., Ku znetsova, M., Hesse, M., Ridley, A., Raeder, J., Singer, H. J., and Chulaki, A.: Systematic evaluation of ground and geostationary magnetic field predictions generated by global magnetohydrodynamic models, J. Geophys. Res., 115, A03206, doi:10.1029/2009JA014537, 2010.

Raeder, J., McPherron, R. L., Frank, L. A., Kokubun, S., Lu, G., Mukai, T., Paterson, W. R., Sigwarth, J. B., Singer, H. J., and Slavin, J. A.: Global simulation of the Geospace Environment Modeling substorm challenge event, J. Geophys. Res., 106, 381–395, 2001.

Rastätter, L., Kuznetsova, M. M., Vapirev, A., Ridley, A., Wiltberger, M., Pulkkinen, A., Hesse, M., and Singer, H. J.: Geospace Environment Modeling 2008–2009 Challenge: Geosynchronous magnetic field, Adv. Space Res., 9, S04005, doi:10.1029/2010SW000617, 2011.

Riazantseva, M. O., Dalin1, P. A., Zastenker, G. N., and Richardson, J.: Orientation of sharp fronts of the solar wind plasma, Cosmic Res.+, 41, 405–416, 2003.

Shi, Y., Zesta, E., and Lyons, L. R.: Features of energetic particle radial profiles inferred from geosynchronous responses to solar wind dynamic pressure enhancements, Ann. Geophys., 27, 851–859, doi:10.5194/angeo-27-851-2009, 2009.

Schwartz, S. J., Chaloner, C. P., Christiansen, P. J., Coates, A. J., Hall, D. S., Johnstone, A. D., Gough, M. P., Norris, A. J., Rijnbeek, R. P., Southwood, D. J., and Woolliscroft, Les J. C.: An

active current sheet sheet in the solar wind, Nature, 318, 269–271, 1985.

Sibeck, D. G., Kudela, K., Lepping, R. P., Lin, R., Nemecek, Z., Nozdrachev, M. N., Phan, T.-D., Prech, L., Safrankova, J., Singer, H., and Yermolaev, Y.: Magnetopause motion driven by interplanetary magnetic field variations, J. Geophys. Res., 105, 25155–25169, 2000.

Sibeck, D. G., Phan, T.-D., Lin, R., Lepping, R. P., and Szabo, A.: Wind observations of foreshock cavities: A case study, J. Geophys. Res., 107, 1271, doi:10.1029/2001JA007539, 2002.

Sun, T. R., Wang C., Li H., and Guo, X. C.: Nightside geosynchronous magnetic field response to interplanetary shocks: Model results, J. Geophys. Res., 116, A04216, doi:10.1029/2010JA016074, 2011.

Tsyganenko, N. A.: A model of the near magnetosphere with a dawn-dusk asymmetry – 1. Mathematical structure, J. Geophys. Res., 107, 1179, doi:10.1029/2001JA000219, 2002.

Tsyganenko, N. A. and Stern D. P.: Modeling the global magnetic field of the large-scale Birkeland current systems, J. Geophys. Res., 101, 27187–27198, doi:10.1029/96JA02735, 1996.

Turner, D. L. and Li, X. L.: Radial gradients of phase space density of the outer radiation belt electrons prior to sudden solar wind pressure enhancements, Geophys. Res. Lett., 35, L18101, doi:10.1029/2008GL034866, 2008.

Villante, U. and Piersanti, M.: An analysis of sudden impulses at geosynchronous orbit, J. Geophys. Res., 113, A08213, doi:10.1029/2008JA013028, 2008.

Wang, C., Sun, T. R., Guo, X. C., and Richardson, J. D.: Case study of nightside magnetospheric magnetic field response to interplanetary shocks, J. Geophys. Res., 115, A10247, doi:10.1029/2010JA015451, 2010.

Wiltberger, M., Pulkkinen, T. I., Lyon, J. G., and Goodrich C. C.: MHD simulation of the magnetotail during the December 10, 1996, substorm, J. Geophys. Res., 105, 27649–27663, 2000.

Yu, Y and Ridley, A. J.: The response of the magnetosphere-ionosphere system to a sudden dynamic pressure enhancement under southward IMF conditions, Ann. Geophys., 27, 4391–4407, doi:10.5194/angeo-27-4391-2009, 2009.

Yue, C., Zong, Q. G., Zhang, H., Wang, Y. F., Yuan, C. J., Pu, Z. Y., Fu, S. Y., Lui, A. T. Y., Yang, B., and Wang, C. R.: Geomagnetic activity triggered by interplanetary shockst, J. Geophys. Res., 115, A00I05, doi:10.1029/2010JA015356, 2010.